A "no-flow-sensor" wind estimation algorithm for unmanned aerial systems

Stéphanie Mayer, Gautier Hattenberger, Pascal Brisset, Marius Jonassen, Joachim Reuder

A 'no-flow-sensor' Wind Estimation Algorithm for Unmanned Aerial Systems

Stephanie Mayer, Gautier Hattenberger, Pascal Brisset, Marius O. Jonassen and Joachim Reuder

Reprinted from

International Journal of
Micro Air Vehicles

Volume 4 · Number 1 · March 2012

Multi-Science Publishing
ISSN 1756-8293

A 'no-flow-sensor' Wind Estimation Algorithm for Unmanned Aerial Systems

Stephanie Mayer[1,3], Gautier Hattenberger[2], Pascal Brisset[2], Marius O. Jonassen[1] and Joachim Reuder[1]

[1]Geophysical Institute, University of Bergen, Allegaten 70, 5007 Bergen, Norway
[2]Ecole Nationale de l'Aviation Civil, 7, avenue Edouard Belin, 31055 Toulouse Cedex 4, France
[3]now at: Bjerknes Centre for Climate Research,
Allegaten 70, 5007 Bergen, Norway
Tel.: +47-55 58 87 13, Fax: +47-55 58 98 83, Email: stephanie.mayer@uni.no

ABSTRACT

A 'no-flow-sensor' wind estimation algorithm for Unmanned Aerial Systems (UAS) is presented. It is based on ground speed and flight path azimuth information from the autopilot's GPS system. The algorithm has been tested with the help of the simulation option in the Paparazzi autopilot software using artificial wind profiles. The retrieval accuracy of the predefined profiles by the wind algorithm and its sensitivity to vertical aircraft velocity, diameter of the helical flight pattern and different data sampling methods have been investigated. The algorithm with a correspondingly optimized set of parameters is then applied to various scientific flight missions under real wind conditions performed by the UAS SUMO (Small Unmanned Meteorological Observer). The SUMO wind profiles are compared to measurements of conventional atmospheric profiling systems as radiosondes and piloted balloons. In general, the presented 'no-flow-sensor' wind estimation method performs well in most atmospheric situations and is now operationally used in the post-processing routine for wind profile determination from SUMO measurements.

Keywords: 'no-flow-sensor' wind estimation; Paparazzi autopilot system; Small Unmanned Meteorological Observer SUMO; atmospheric measurements;

1. INTRODUCTION

Further progress in atmospheric modeling, important for improved weather forecasts and reliable future climate projections, is inevitably linked to the availability of appropriate data sets for model initialization, model test and validation, and finally model improvement [1, 2, 3]. It is well known that a large portion of the existing model uncertainties can be attributed to an incomplete and unsatisfactory description of relevant atmospheric processes in the atmospheric boundary layer (ABL), i.e., the lowest few kilometers in the atmosphere [4, 5]. As this lower part of the atmosphere is easily accessible by UAS, such systems provide a vast potential to increase the corresponding observational capabilities. Enabling atmospheric profiling and horizontal surveys of the meteorological key variables pressure, temperature, humidity and wind, in unique spatial and temporal resolution, UAS are expected to be an ideal tool to close the existing observational gap between ground based measurements (e.g. synoptic meteorological network, measurement masts) and satellite observations.

The use of relatively small and therefore cost-efficient UAS as an alternative to conventional meteorological profiling systems (e.g. radiosondes (see Section 5)) in meteorological field campaigns has become more frequent and manifold. Konrad [6] pioneered within this field in the early 1970s with an instrumented and remotely piloted model aircraft. A similar profiling system (KALI), has been developed at the University of Munich in the late 1990s. It has been operated during various field experiments in Nepal, Bolivia and Germany up to 3 km above the ground, in particular for the investigation of orographic effects on atmospheric flow [7, 8]. Two significant shortcomings of the KALI system are the need of experienced pilots for continuous remote controlled operation of the aircraft and the lack of an appropriate wind measurement system.

Technical progress and electronic miniaturization has triggered the development of UAS equipped with autopilot systems during the last decade (e.g. [9]). Examples for successful application of this concept for atmospheric research are among others, the Aerosonde built in Australia [10], the M^2AV developed in Germany [11], and the Small Unmanned Meteorological Observer (SUMO) [12], developed under the auspices of the Geophysical Institute, University of Bergen in Norway. The larger of these systems have a typical payload of a few kilograms. Therefore it is possible to carry a set of sensors for the determination of the meteorological wind speed. The true air speed (TAS) measured by any kind of flow sensor on the airframe can be transformed into the wind speed (u) when the ground speed (GS) and the aircraft's attitude, i.e., the Eulerian angles (yaw, pitch, roll), are known (e.g. [13] and [14]). Small UAS, such as SUMO, have strictly limited payload capacities in the order of some tens of grams. Thus, the development of an alternative wind estimation method, without the need of direct flow measurement, but with an accuracy comparable to that of standard profiling systems such as radiosondes (systematic bias: 0.2 m/s; random error: 0.6-3 m/s [15]), is required for small and lightweight platforms.

The SUMO system has been designed and developed in cooperation between the Geophysical Institute at the University of Bergen, Norway, Martin Müller Engineering, Germany and the UAS laboratory at ENAC in Toulouse, France. Main design criteria were the capability of determining meteorological variables such as pressure, temperature, humidity, wind speed and wind direction with satisfactory accuracy in addition to mobility, flexibility, cost-efficiency and low infrastructural demands for measurements in remote areas. The system is intended to be operated as a 'controllable and recoverable radiosonde' inside and above the ABL. This way, it will help to close the existing gap of in-situ ABL observations covering horizontal scales from several tens of meters up to around 10 km. The SUMO UAS system in its current version ([12] and [16]) is based on a modification of the FunJet construction kit by Multiplex. It has a wingspan of 80 cm and an overall take-off weight of 580 g (see Figure 1a). It is electrically powered by a lithium polymer battery (3 cells, 11.1 V, capacity 2600 mAh) driving a pusher-propeller by a 140 W motor in the rear of the airframe. SUMO has a typical endurance of 20 minutes full power motor time, enabling flight missions up to about one hour. For autonomous flight capabilities SUMO is equipped with the Paparazzi autopilot system ([17] and http://paparazzi.enac.fr/wiki/Overview). Paparazzi is an open source autopilot hardware and software project mainly dedicated to the operation of small fixed and rotary wing UAS. It includes the ground control station (GCS) for operation and pre-flight mission planning and simulation (see Figure 1b). Bi-directional data communication between GCS and aircraft, both for online data transfer to the ground and in-flight mission modification toward the aircraft is implemented by a 2.4 GHz telemetry link. SUMO can easily be used in remote areas without extensive infrastructure. During the last years it has been operated during several field campaigns and successfully performed nearly 700 scientific flight missions (e.g. [12] and [18]). By that it has proven its great value, e.g. for the evaluation of fine scale numerical weather prediction (NWP) models [19].

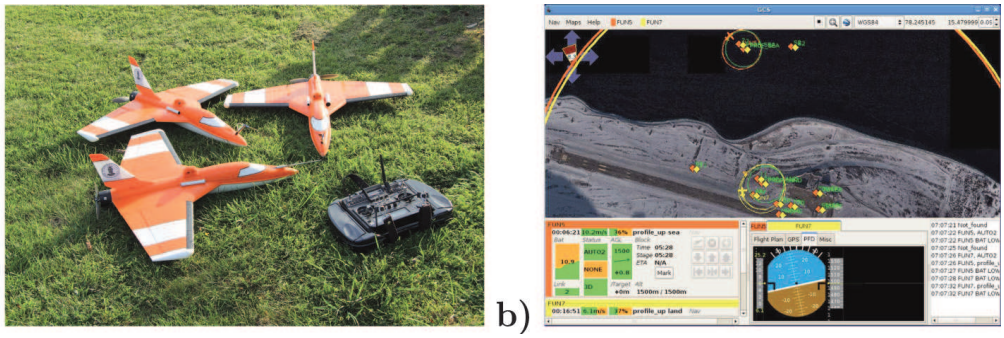

a) b)

Figure 1. a) Fleet of SUMOs and a remote control; b) a screenshot of the ground control station (GCS) during flight.

The 'no-flow-sensor' wind estimation algorithm is introduced in the following Section 2. Paparazzi simulations for testing the method in specific wind conditions are described in Section 3 with the aim to optimize the combination of flight pattern and algorithm parameter configuration. In Section 4, the

wind algorithm is tested against simulations for a real föhn situation. Followed by Section 5 where these configurations are applied in the algorithm for the determination of real wind profiles. These wind estimations are compared to conventional atmospheric profiling systems, such as piloted balloon (PiBal) and radiosonde (RaSo) measurements. Finally the study is summarized in Section 6. A short outlook is given in Section 7.

2. WIND ESTIMATION ALGORITHM

2.1 Description

The wind triangle sketched in Figure 2 describes the wind impact on a flying aircraft. By measuring the true air speed vector (**TAS**) and the ground speed vector (**GS**) of the aircraft, the atmospheric wind (**u**) can be determined (e.g. [13] and [14]). This implies that both variables have to be measured with very high accuracy since they usually are of greater magnitude than the variable that has to be calculated. Therefore, sophisticated TAS and Eulerian angle measurement equipment consisting of at least a flow sensor and gyroscope is necessary for a direct wind measurement by using the wind triangle method. As small UAS have a very limited payload capacity, alternative ways for the determination of the horizontal wind have to be developed. In the 'no-flow-sensor' wind estimation method only onboard GPS information (time (t), height above ground (z), flight-path azimuth (χ) and ground speed (GS)) is used to estimate wind speed and wind direction.

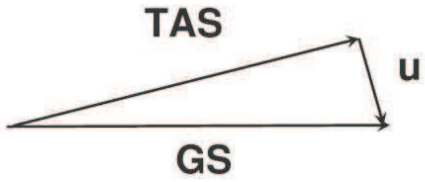

Figure 2. A vector diagram of the wind triangle. TAS: true airspeed, GS: ground speed and u: horizontal wind.

Before the algorithm is explained in detail, some basic variables have to be defined. The 'no-flow-sensor' method implies a helical (for vertical profiles) or a circular (for horizontal surveys) flight pattern. During flight in a circle the aircraft is influenced by the horizontal wind, experiencing tailwind it flies faster while it is slowed down in headwind conditions. A corresponding ground speed distribution along the flight track is shown in Figure 4.

The wind triangle (Figure 2) is formulated as:

$$\mathbf{TAS} + \mathbf{u} = \mathbf{GS} \tag{1}$$

The mean of the TAS can be calculated by

$$\overline{TAS} = \frac{1}{N}\sum_{i}^{N} \|\mathbf{GS_i} - \mathbf{u}\|. \tag{2}$$

The corresponding variance and standard deviation are defined as:

$$\sigma^2_{TAS} = \frac{1}{N}\sum_{i}^{N} \left(\|\mathbf{GS_i} - \mathbf{u}\| - \overline{TAS}\right)^2 \tag{3}$$

$$\sigma^2_{TAS} = \frac{1}{N}\sum_{i}^{N} \left(\|\mathbf{GS_i} - \mathbf{u}\| - \overline{TAS}\right)^2 \tag{4}$$

For the initialization of the algorithm, the horizontal wind **u** is set to [0,0], i.e., **TAS** = **GS**. Flying the aircraft with constant throttle and pitch angle, nearly constant **TAS** can be assumed. A way to visualize the wind algorithm is to project **GS** and **TAS** in a Cartesian plane. The algorithm fits a circle through the measurement points (see Figure 3). The circle is found by minimizing the distances (σ_{TAS}) between the measurement points to fit a circle sector with radius r = TAS. This can be achieved by applying a minimization algorithm such as the Nelder-Mead method [20]. This method is known for its computational efficiency and robustness. It is a simplex method for finding a local minimum of a function of several variables. For two variables, a simplex is a triangle, and the method is a pattern search that compares function values at the three vertices of a triangle. The worst vertex, i.e., the largest function value, is rejected and replaced with a new vertex. A new triangle is formed and the search is continued. The process generates a sequence of triangles (which can have different shapes), for which the function values at the vertices decrease. The size of the triangles is reduced and the coordinates of the minimum point are found. The algorithm is stated using the term simplex (a generalized triangle in n dimensions) and will find the minimum of a function of n variables [21]. In the example sketched in Figure 3 a circle with a radius of $TAS \approx 18$ is found. By using the GPS measurement of **GS** = [GS sin(χ), GS cos(χ)] the wind can finally be estimated by the vector difference between **GS** and **TAS**, resulting in **u** = (4.8, 0)) in Figure 3.

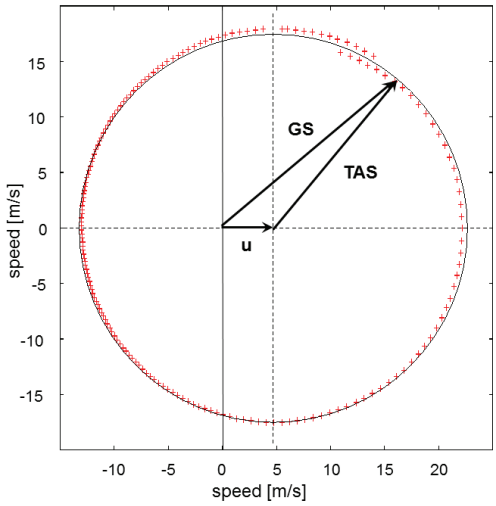

Figure 3. An example of GPS output (red crosses) projected into the Cartesian plane. The black line represents a fit to the respective ground speed values.

3. SIMULATIONS

The Paparazzi software incorporates a flight simulation module. This tool has been used to test the algorithm by pre-describing artificial wind conditions. Two different synthetic wind profiles have been applied:

1. constant wind speed $|\mathbf{u}|$ = ws = 10 m/s from 0 to 2000 m above ground level (agl) and veering (clockwise changing) wind direction with height covering the entire range of 0° to 360° (see Figure 5a).
2. constant wind direction (wd = 270°), and changing wind speed with height (see Figure 5b)).

The reason for choosing these wind conditions is first of all to clarify if the wind algorithm can cope correctly with all possible wind directions and secondly to see how appropriate it is for the resolution of vertical wind speed gradients (wind shears) changing sharply as indicated in Figure 5b in z = 1500 m agl.

Both artificial wind profiles have been combined with different flight parameters, such as helix radius and climb speeds, and two different data sampling methods to perform a comprehensive sensitivity study.

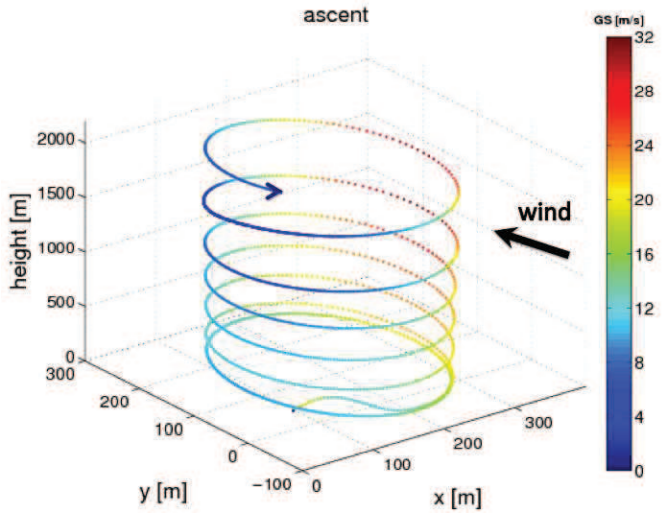

Figure 4. SUMO ascent flight path; color bar indicates the changing GS [m/s] corresponding to the aircraft encountering headwind (GS small, blue colors) and tailwind (GS high, red colors).

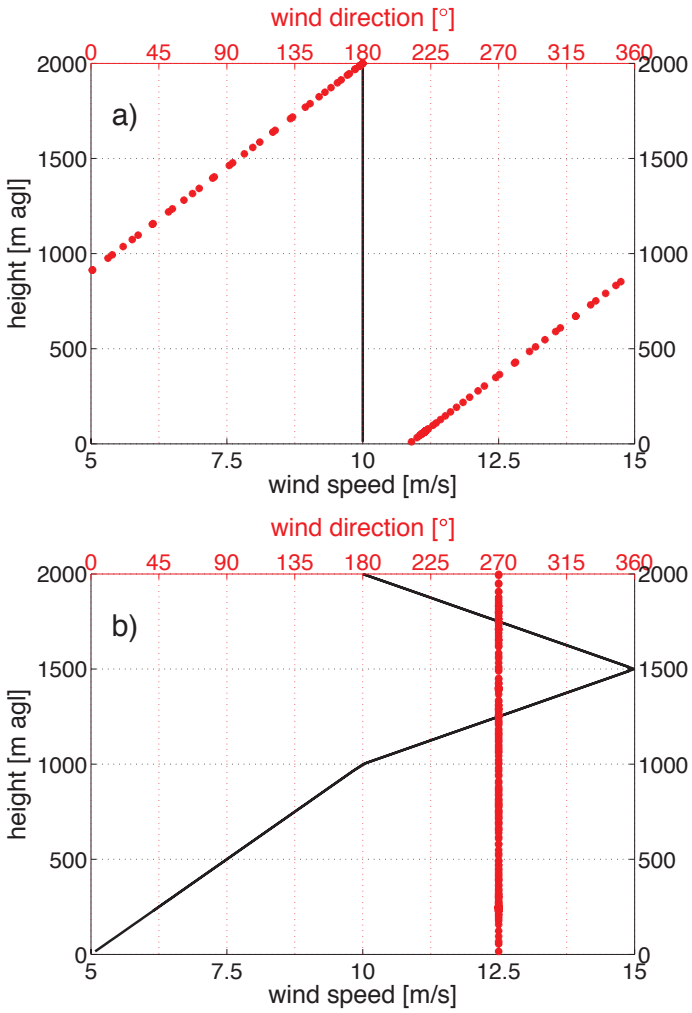

Figure 5. Synthetic wind functions used as test references. Bottom axes: wind speed. Top axes: wind direction. a) twisted wind profile with constant wind speed. b) constant wind direction profile with changing wind speed with height.

3.1 Flight parameters

For ABL studies it is desirable to profile the whole depth of the ABL and even to penetrate capping inversions which can typically reside in heights of 500 m to 2000 m agl. In its current version, the SUMO aircraft motor run time is limited by the battery capacity to approximately 20 min, i.e., with a climb speed of 5 m/s it can reach approximately 3000 m and return safely back to ground. In practice, SUMO climbs in a helix with a radius (r) in the order of 100-200 m (see Figure 4) with a climb speed (cs) ranging between 2 to 8 m/s. Accordingly, the algorithm has been tested for a helix with r_1 = 120 m and r_2 = 200 m, and for cs_1 = 2 m/s, cs_2 = 4 m/s, and cs_3 = 8 m/s.

3.2 Data sampling methods

Two data sampling methods are applied, one representing spatial sampling (1.), the other one temporal sampling (2.):

1. The spatial samples $N = i...n$ are taken for single angular slots (α). Slots of α = 5°, α = 10° and α = 15° have been used.
2. The temporal samples $N = i...n$ are taken over a specific time period (p). Periods of p = 60 s, p = 90 s and p = 120 s have been applied.

Mean height intervals Δz are calculated by averaging heights z_i within each sample.

3.3 Quality tests

As an objective measure of which method is preferable, the average of the root mean squared error ($\bar{\delta}$) is calculated for each configuration:

$$\delta = \sqrt{\frac{1}{n}\sum(t_i - s_i)^2} \tag{5}$$

t: truth and s: simulation. index $i...n$: measurements.

Tables 1-4 summarize the results of the performed sensitivity study. Tables 1 and 2 correspond to the quality of determined wind speed and wind direction using the artificial wind profile 1 (constant wind speed, constant change of wind direction with height). Tables 3 and 4 show the results for wind profile 2 (constant wind direction, continuous wind shear with a maximum wind speed at 1500 m above ground). The results for the wind speed in case 1 (Table 1) show in general a high sensitivity of the retrieval quality to climb speed. The higher the climb speed, the larger $\bar{\delta}(ws)$. The sensitivity to climb speed is more pronounced for the temporal sampling. The results also indicate a general increase in $\bar{\delta}(ws)$ toward larger r. The quality of the spatial method seems to be nearly independent of the choice of the angular slot size α for the probed sector. These findings are confirmed by the results of the wind speed retrieval for case 2. The only difference is the slightly reduced sensitivity of the temporal method with respect to climb speed and radius of the helical flight path. For the wind direction (Table 2 and 4) the situation is not as clear. Again there is in most cases an increase in $\bar{\delta}(wd)$ with climb speed, except for the spatial method in case 2, where the 8 m/s simulation shows a slightly decreased root mean squared error $\bar{\delta}(wd)$).

Overall, the 'no-flow-sensor' wind estimation algorithm performs very well in the parameter space of the conducted simulations. $\bar{\delta}(ws)$ is distinctly below 1 m/s, except for some simulations with the 8 m/s climb speed. $\bar{\delta}(wd)$ remains nearly always below 5°. With this, the algorithm is expected to enable the determination of wind profiles with an accuracy that is comparable to other in-situ wind profiling methods. From the presented sensitivity study alone, no clear advice for the preferable use of the spatial or temporal sampling method can be given. Anyway, it is clear that low climb speeds should be favored. Low climb speeds are, however, rather inefficient for reaching high ceiling altitudes required e.g. for a comprehensive profiling of daytime convective boundary layers that can extend vertically over more than 2 km above ground. In such cases, SUMO is therefore typically operated with high and very efficient climb rates of 8-10 m/s during ascent, but rather low vertical velocities in the order of 2 m/s during descent.

Table 1. Average of root mean squared errors ($\bar{\delta}(ws)$) in m/s and corresponding percentage errors (e) for the simulations based on the wind speed profile shown in Figure 5a. Tested are the estimation methods (spatial method, temporal method) and helix size (r = 120 m, r = 200 m) for different climb speeds (cs).

	cs [m/s]	spatial [°]					temporal [s]				
		5	10	15	avg.	[%]	60	90	120	avg.	e [%]
120 m	± 2	0.31	0.31	0.32	**0.31**	**3.1**	0.27	0.25	0.22	**0.24**	**2.4**
	± 4	0.36	0.37	0.38	**0.37**	**3.7**	0.28	0.44	0.69	**0.47**	**4.7**
	± 8	0.63	0.65	0.67	**0.65**	**6.5**	0.84	1.57	2.62	**1.68**	**16.8**
200 m	± 2	0.35	0.36	0.37	**0.36**	**3.6**	0.52	0.34	0.34	**0.40**	**4.0**
	± 4	0.52	0.52	0.54	**0.53**	**5.3**	0.57	0.64	0.81	**0.67**	**6.7**
	± 8	1.22	1.23	1.23	**1.23**	**12.3**	1.69	1.84	2.93	**2.15**	**21.5**

Table 2. Average of root mean squared errors ($\bar{\delta}(ws)$) in degrees (°) for the simulations based on the wind direction profile shown in Figure 5a.

	cs [m/s]	spatial [°]				temporal [s]			
		5	10	15	avg.	60	90	120	avg.
120 m	± 2	2.16	2.21	2.35	**2.24**	0.90	1.21	1.04	**1.05**
	± 4	2.81	2.88	2.96	**2.88**	1.56	1.59	2.01	**1.72**
	± 8	5.89	7.06	4.10	**5.68**	2.50	2.34	3.46	**2.77**
200 m	± 2	2.33	2.48	2.54	**2.45**	2.58	2.09	1.87	**2.18**
	± 4	3.54	3.61	3.65	**3.60**	4.90	1.84	4.09	**3.61**
	± 8	4.02	4.04	4.10	**4.05**	8.29	2.34	3.21	**4.61**

Table 3. Average of root mean squared errors ($\bar{\delta}(ws)$) in m/s and corresponding percentage errors (e) for the simulations based on wind speed shown in Figure 5b.

	cs [m/s]	spatial [°]					temporal [s]				
		5	10	15	avg.	e [%]	60	90	120	avg.	e [%]
120 m	± 2	0.54	0.51	0.51	**0.52**	**5.0**	0.43	0.43	0.44	**0.43**	**4.1**
	± 4	0.55	0.45	0.51	**0.50**	**4.8**	0.54	0.54	0.57	**0.55**	**5.5**
	± 8	0.90	0.88	0.73	**0.84**	**8.1**	0.70	0.81	0.97	**0.83**	**8.0**
200 m	± 2	0.36	0.49	0.42	**0.42**	**4.0**	0.87	0.40	0.39	**0.55**	**5.5**
	± 4	0.91	0.89	0.91	**0.90**	**8.7**	0.75	0.58	0.61	**0.65**	**6.3**
	± 8	1.04	0.95	0.90	**0.96**	**9.2**	0.82	0.82	0.95	**0.86**	**8.3**

Table 4. Root mean squared differences ($\bar{\delta}(ws)$) in degrees (°) for the simulations based on wind direction shown in Figure 5b.

	cs [m/s]	spatial [°]				temporal [s]			
		5	10	15	avg.	60	90	120	avg.
120 m	± 2	2.55	2.53	2.58	**2.55**	2.37	2.23	2.19	**2.26**
	± 4	2.37	2.48	2.59	**2.48**	1.84	1.86	1.88	**1.86**
	± 8	1.89	1.89	1.93	**1.90**	2.34	2.29	2.29	**3.31**
200 m	± 2	1.77	1.82	2.25	**3.73**	2.86	2.23	2.86	**3.15**
	± 4	3.02	2.95	2.66	**2.88**	4.41	3.31	3.42	**3.71**
	± 8	4.71	4.76	4.70	**4.72**	5.20	5.06	4.98	**5.08**

4. SIMULATION OF A 'FÖHN' CASE

The wind conditions applied in Section 3 are rather artificial. In the next step, the algorithm has also been tested in a simulation based on real wind conditions. For this case, a 'föhn' wind situation has been selected. The föhn wind is a dry down-slope wind occuring on the lee side of the Alps. The corresponding simulations have been initialized with a wind profile measured by a radiosonde launched in Munich, Germany on 26.02.2010 at 00 UTC. The shown wind profile is characterized by a nocturnal low-level jet at 250 m above ground, rather constant wind speeds of around 7 m/s between 400 m and 1000 m, and increasing wind speeds above, reaching a maximum wind speed of 15 m/s at 1800 m agl. Aloft, the wind is slightly decreasing to 12 m/s at 3000 m agl. The wind direction is mostly westerly with a slight turn to southerly directions in 1000 to 1500 m agl (see Figure 6).

The resulting wind profiles derived by the wind algorithm are shown in Figure 6a for the temporal (p = 60 s) and in Figure 6b for the spatial sampling method ($\alpha = 5°$). The color indicates the simulations for ascent light gray) and descent (dark gray). In general, the wind estimation algorithm reproduces the initial profile very well. At altitudes below 1300 m both sampling methods fit the initial profile excellent, with an overall better score for the spatial sampling method. The root mean squared error for both sampling methods are $\bar{\delta}(ws) = 2.16$ for the temporal method respectively $\bar{\delta}(ws) = 0.65$ for the spatial method. With higher ambient wind speeds above 1300 m, the temporal sampling method seems to get unstable, resulting in distinct spikes around the measured profile. These are the result of the increasing wind at this altitude reaching nearly the TAS of the aircraft. Looking at a selection of GPS positions during descent, numerous oscillations can be identified, when the aircraft is impacted by strong headwind (see Figure 7). The spatial sampling method shown in Figure 6b does not produce such outliers under headwind conditions. This can be explained by the fact that the temporal data sampling method cannot find an appropriate matching circle due to the aircrafts flight path oscillations while the spatial sampling method overcomes this issue.

5. ATMOSPHERIC MEASUREMENTS

In meteorology, well established in-situ measurement platforms for wind profiles are e.g. radiosondes (RaSo). A radiosonde or rawinsonde is a measurement unit that is attached to a helium filled weather balloon (see Figure 8). To date, radiosondes are normally equipped with a temperature, humidity and pressure sensor and a GPS device. They can penetrate the troposphere and reach high altitudes (> 25 km). Radiosondes are influenced by local wind conditions and therefore they can be quickly blown away from their launch position. Usually they cannot be recovered and thus, they are a rather expensive tool when frequently used. An alternative tool to determine wind speed and wind direction is the method of piloting a small helium filled balloon (PiBal) simultaneously with two theodolites (shown in Figure 9), see e.g. [22]. To investigate the quality of wind profile derivation by the 'no-flow-sensor' wind algorithm in comparison with these conventional in-situ profiling measurement tools, SUMO has been operated in parallel with the aforementioned measurement platforms in several field campaigns. The results are summarized in Table 5. Again both sampling methods have been applied. For the spatial sampling method, we have chosen a slot of $\alpha = 5°$ and for the temporal sampling method, we have used a period of p = 60 s.

Table 5. Average of root mean squared errors ($\overline{\delta}(ws)$) of the measured wind speed (ws) and wind direction (wd). Wind conditions are indicated in m/s in the right column.

profiles	$\overline{\delta}$**(ws)**		$\overline{\delta}$**(wd)**		**wind speed**
	temporal	spatial	temporal	spatial	m/ s
Iceland, 2007 (Figure 10)	39.02	2.55	40.98	25.51	< 5
Svalbard, 2008 (Figure 11)	1.71	1.04	10.82	5.42	10-15
Germany, 2008 (Figure 12)	1.53	1.10	21.07	10.36	5-10
Norway, 2009 (Figure 13)	1.92	1.56	9.51	5.46	10-15

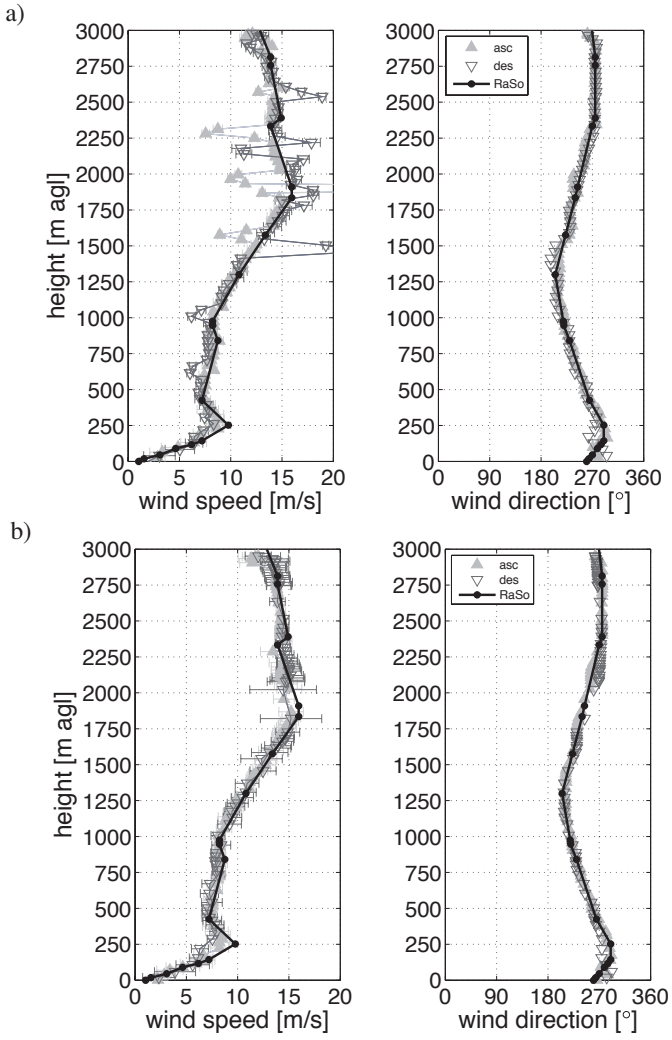

Figure 6. A radiosonde wind profile for a 'föhn' case in Munich, Germany, 26.02.2010 00:00 UTC. a) temporal method has been used. b) using the spatial sampling method. Black line: radiosonde (RaSo); light gray: ascent (asc); dark gray: descent (des).

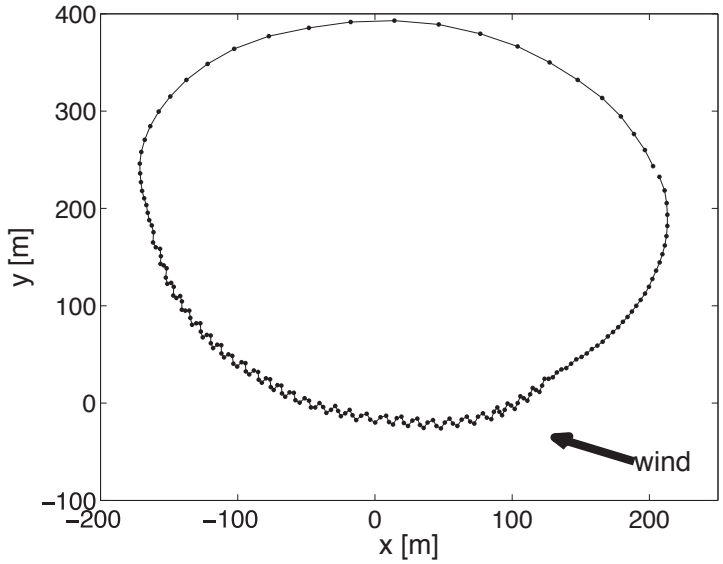

Figure 7. SUMO positions in x-y plane during strong wind conditions. The flight direction is counter-clockwise.

Figure 8. Launch of a radiosonde (RaSo) from the coast guard vessel KV Svalbard.

Figure 9. Piloted balloon measurements.

Figure 10 displays a comparison between PiBal measurement (black line) and a SUMO profile where both the temporal (light gray line) and spatial (dark gray line) method have been applied. The PiBal profile is in this case temporally lagged by one hour to the SUMO flight. Both systems show low wind speeds in the order of 2-5 m/s from westerly directions. SUMO data have been averaged between ascent and descent. To enable the direct comparison between both sounding systems, both data sets have been averaged in 50 m height intervals. Both methods show almost identical results in heights z ≥ 400 m. Low wind speed (≤ 5 m/s) from westerly to southwesterly directions. Considering PiBal data representing the true state of the atmosphere, the spatial method reduces the root mean squared errors ($\overline{\delta}$) both for wind speed and wind direction quite substantially. The spatial method performs well in low heights (≤ 400 m) compared to the temporal method which fails in this case in heights z < 400 m where SUMO had to leave its helical flight pattern due to switch to manual mode.

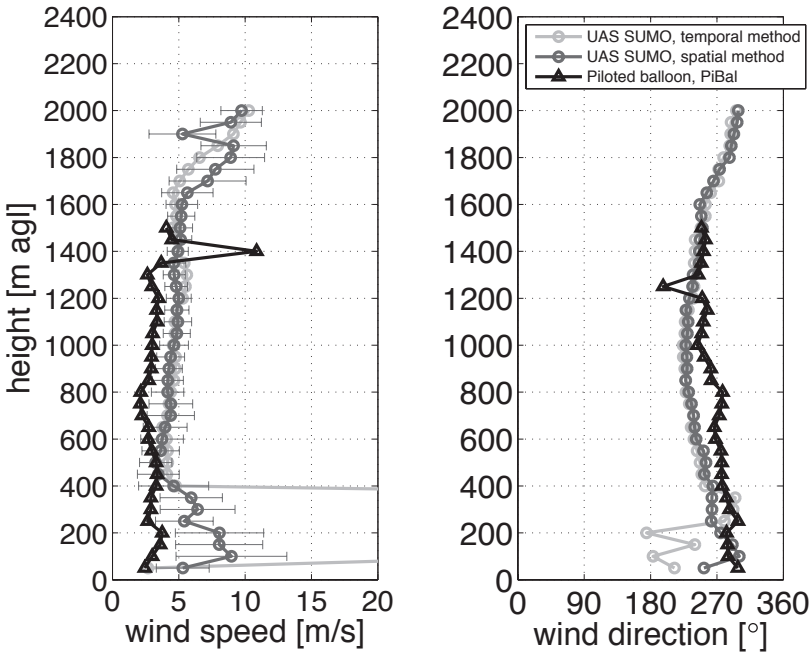

Figure 10. A measured wind profile in Central Iceland, 18.08.2007 17:56 UTC. Black triangles: piloted balloon (PiBal) measurements; light gray circles: wind algorithm using the temporal sampling method with p=60 s; dark gray circles: wind algorithm using the spatial sampling method with α = 5°. The errorbars indicate the mean standard deviation for each data samples.

Figure 11 shows SUMO wind estimations in comparison to a RaSo measurement. Both systems have been launched simultaneously from the Norwegian coast guard vessel KV Svalbard. The RaSo sounding registered wind speeds of 15 m/s from northeast in heights of 200 to 600 m above ground. Above, the wind speed decreased to 10 m/s and turned slightly to more easterly directions. The SUMO sounding corresponds very well with the RaSo wind measurement both in wind speed and wind direction. Again, considering the RaSo representing the truth, the spatial method reduces the $\overline{\delta}$ for wind speed (ws) by ca. 40 % and for the wind direction (wd) by 50 % compared to the temporal method. Figure 12 presents another example of a SUMO wind profile simultaneously measured with a RaSo ascent in Coburg, Germany. The RaSo measured wind speeds between 6-11 m/s with two minima; one at 200 m agl and a second one at 1000 m agl. A wind speed maximum can be identified in 1400 m agl. Overall, the SUMO measurement matches well with the RaSo. The spatial method reduces $\overline{\delta}(ws)$ by approximately 30 %. The wind direction ranges between southeast and east. The SUMO measurement agrees also well with the RaSo measurement. The spatial method reduces $\overline{\delta}(wd)$ by ca. 50 %.

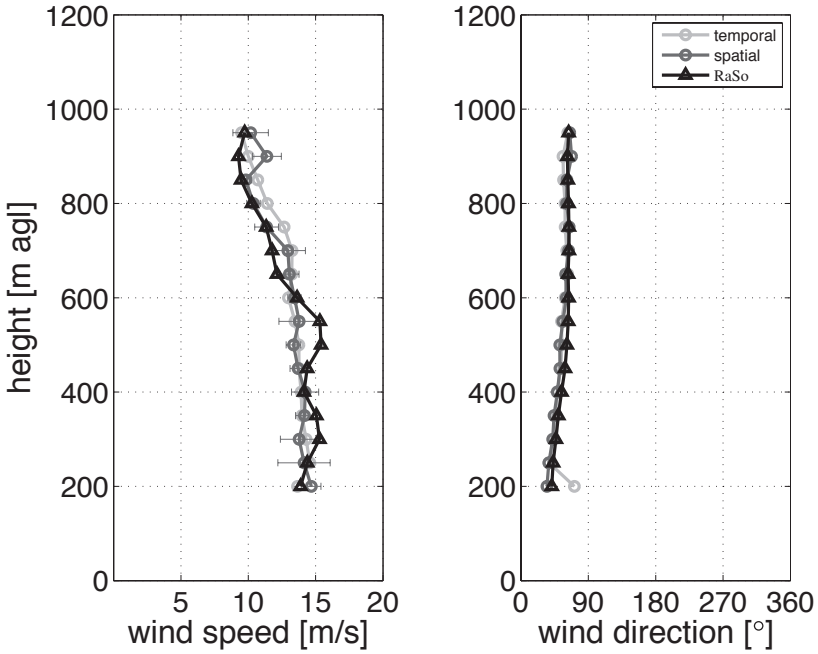

Figure 11. A measured wind profile on Svalbard, 28.02.2008 15:11 UTC. Color code as in Figure 10.

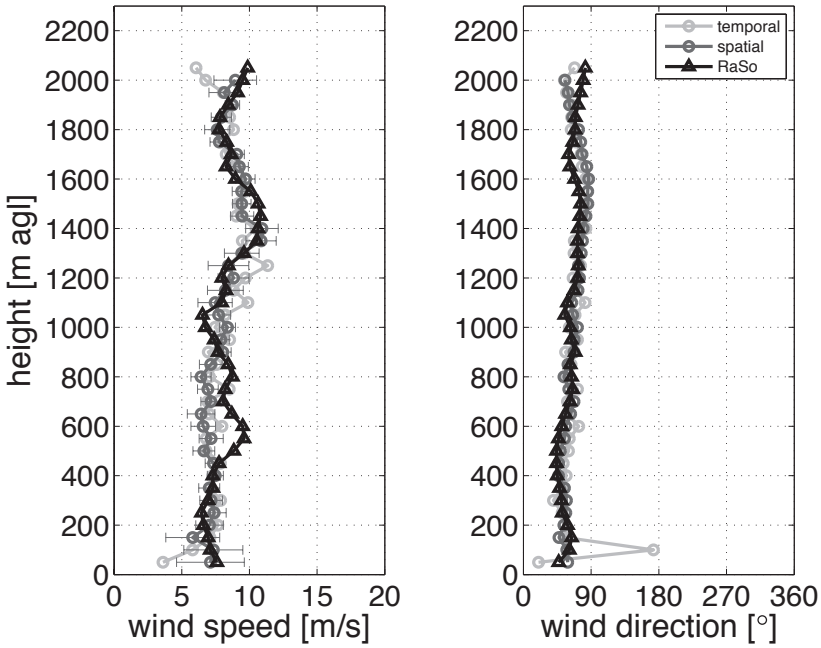

Figure 12. A measured wind profile at Coburg, Germany, 24.07.2008 12:00 UTC. Color code as in Figure 10.

Figure 13 shows another example of quite strong wind conditions of 8 to 14 m/s measured from the Norwegian coast guard vessel KV Harstad in Andfjorden, Northwestern Norway. The wind speed is almost linearly increasing with height. In this case, SUMO measurements show wind speeds that are in average 1-2 m/s lower compared to the RaSo. This is most likely due to the time lag of almost 2 hours between both launches. Additional discrepancies in the compared wind data can be expected due to the increasing horizontal separation of both systems with altitude, as SUMO is profiling stationary while the RaSo is drifting with the wind. Again, the spatial sampling method reduces $\bar{\delta}(ws)$ by ca. 20 %. The

wind direction was mainly west, southwest in lower heights. Both wind direction profiles agree very well. The slots method reduces $\bar{\delta}(wd)$ by approximately 40 %.

Overall, we can state that the spatial sampling method improves the algorithm's performance compared to the temporal sampling method in real wind conditions. This is especially seen for measurements in lower heights. In particular, it is quite crucial because thereby reliable wind information can be gained also at lower levels. Using the temporal sampling method, wind data below 200 m would have to be discarded due to poor data quality (high $\bar{\delta}$).

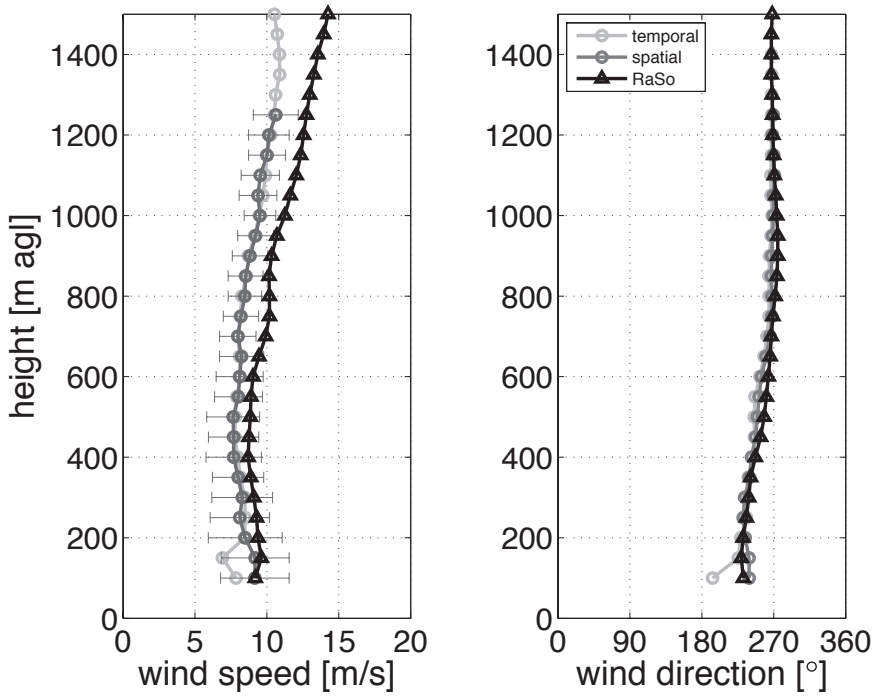

Figure 13. A measured wind profile in Andfjorden, Northern Norway, 27.09.2009 08:28 UTC. Color code as in Figure 10.

6. SUMMARY

In this paper, a 'no-flow-sensor' wind estimation method especially suited for small UAS has been introduced. The algorithm has been tested for different atmospheric conditions by comparing it to simulations and atmospheric measurements. It has been shown that the method can be successfully applied in real atmospheric conditions and that it is appropriate in particular for use with the UAS SUMO. The algorithm has been tested in several configurations, using two different sampling methods (temporal and spatial) as well as different helix radii (120 m and 200 m) and climb speeds (2, 4, 8 m/s). One important outcome is that best wind data quality can be achieved by operating SUMO with low climb speed. As low climb speed is rather inefficient in reaching high ceiling levels for ABL profiling, SUMO is for this purpose typically operated with high vertical velocity during ascent (8-10 m/s) but distinctly lower values (around 2 m/s) during descent.

The comparison of SUMO wind measurements with piloted balloon, and radiosonde measurements, shows clearly that under real atmospheric conditions the spatial method performs significantly better than the temporal period method, especially for low heights above the ground level. The reason for this is that the spatial method is less sensitive to an exact helical flight pattern compared to the temporal method. Applying the algorithm to a simulation of a föhn case with vertical wind shear showed that the temporal sampling method has its shortcomings in strong headwind conditions when the aircraft's track starts to oscillate. Based on the results of this study the spatial data sampling method used within in the 'no-flow-sensor' wind estimation algorithm has been chosen as an inherent part of the SUMOs data post-processing routine.

7. OUTLOOK

From the meteorological point of view, wind measurements closer to the surface (below 200 m) are very important to enable the identification of wind shears and low-level jets close to the ground, in particular for investigations of the stable polar boundary layer. For this purpose, it is highly desirable to operate SUMO in autonomous mode below that height in future field campaigns. First tests in keeping SUMO in autonomous mode in heights considerably lower than 200 m have given promising results.

The SUMO system is under continuous development. Recently, it has been equipped with an inertia measurement unit (IMU) to extend its application range for operations in cloudy conditions and even inside clouds. A pitot tube and 5-hole probe are under integration at the moment. Information from such flow sensors can in the future be used to improve and complement the performance of the presented 'sensor-less' algorithm for wind determination. The 5-hole probe for 3D flow measurements with 100 Hz sampling rate, will enable investigations of atmospheric turbulence e.g. for measurements in the wake of wind turbines.

ACKNOWLEDGEMENTS

We would like to dedicate this paper to our colleague Pascal Brisset, one of the fathers and main driving forces behind the Paparazzi project, who tragically died in a climbing accident in May 2010. Our gratitude is directed to the pilots Christian Lindenberg and Martin Müller being a credible part during numerous field campaigns during the last years. We thank the FLOHOF team and the crews of KV Svalbard and KV Harstad. Thanks also to the RaSo team of the Meteorological Institute Munich (MIM) for assistance during the field experiment performed in Coburg, Germany. Field grants for M. O. Jonassen and J. Reuder were partly covered by the Arctic Field Grant RiS ID 2902, by the project "Measurement of the energy exchange over sea ice and Arctic leads" (Meltzer foundation, University of Bergen, project number 480627) and IPY/THORPEX (grant number 175992/S30; www.ipythorpex.no). This is publication no. A 377 from the Bjerknes Centre for Climate Research.

REFERENCES

[1] K. Dethloff, C. Abegg, A. Rinke, I. Hebestadt, and V. Romanov, "Sensitivity of Arctic climate simulations to different boundary layer parmeterizations in a regional climate model," *Tellus*, vol. 53A, pp. 1–26, 2001.

[2] D. Stensrud, *Parameterization schemes: Keys to understanding numerical weather prediction models*. Cambridge University Press, pp. 459, 2007.

[3] J. Teixeira, B. Stevens, C. Bretherton, R. Cederwall, J. Doyle, J. Golaz, A. Holtslag, S. Klein, J. Lundquist, D. Randall, A. Siebesma, and P. Soares, "Parameterization of the atmospheric boundary layer: A view from just above the inversion," *Bulletin of the American Meteorological Society*, vol. 89, no. 4, pp. 453–458, 2008.

[4] L. Mart, "Stratified atmospheric boundary layers and breakdown of models," *J. of Theor. Comp. Fluid Dyn.*, vol. 11, pp. 263–280, 1998.

[5] M. Tjernström, M. Žagar, J. Svensson, J. Cassano, S. Pfeiffer, A. Rinke, K. Wyser, K. Dethloff, C. Jones, S. T., and M. Shaw, "Modelling the Arctic Boundary-Layer: An Evaluation of Six Arcmip Regional-Scale Models using Data from the Sheba Project," *Boundary-Layer Meteorology*, vol. 117, no. 2, pp. 337–381, 2005.

[6] T. Konrad, M. Hill, J. Rowland, and J. Meyer, "A Small, Radio Controlled Aircraft As A Platform For Meteorological Sensors," *Appl. Phys. Lab. Tech. Digest*, pp. 11–19, 1970.

[7] J. Egger, S. Bajrachaya, R. Heinrich, P. Kolb, S. Lämmlein, M. Mech, J. Reuder, W. Schäper, P. Shakya, J. Schween, and H. Wendt, "Diurnal Winds in the Himalayan Kali Gandaki Valley. Part III: Remotely Piloted Aircraft Soundings," *Monthly Weather Review*, vol. 130, pp. 2042–2058, 2002.

[8] J. Egger, L. Blacutt, F. Ghezzi, R. Heinrich, P. Kolb, S. Lämmlein, M. Leeb, S. Mayer, E. Palenque, J. Reuder, W. Schäper, J. Schween, R. Torrez, and F. Zaratti, "Diurnal Circulation of the Bolivian Altiplano. Part I: Observations," *Monthly Weather Review*, vol. 133, no. 4, pp. 911–924, 2005.

[9] T. Mueller, "On the Birth of Micro Air Vehicles," *International Journal of Micro Air Vehicles*, vol. 1, no. 1, pp. 1–12, 2009.

[10] G. Holland, P. Webster, J. Curry, G. Tyrell, D. Gauntlett, G. Brett, J. Becker, R. Hoag, and W. Vaglienti, "The Aerosonde Robotic Aircraft: A New Paradigm for Environmental Observations," *Bulletin of the American Meteorological Society*, vol. 82, no. 5, pp. 889–901, 2001.

[11] T. Spiess, J. Bange, M. Buschmann, and P. Vörsmann, "First application of the meteorological Mini-UAV M2AV," *Meteorologische Zeitschrift*, vol. 16, no. 2, pp. 159–169, 2007.

[12] J. Reuder, P. Brisset, M. Jonassen, M. Müller, and S. Mayer, "The Small Unmanned Meteorological Observer SUMO: A new tool for atmospheric boundary layer research," *Meteorologische Zeitschrift*, vol. 18, no. 2, pp. 141–147, 2009.

[13] P. Vörsmann, "Ein Beitrag zur bordautonomen Windmessung," *TU Braunschweig Diss.*, 1984.

[14] A. van den Kroonenberg, T. Martin, M. Buschmann, J. Bange, and P. Vörsmann, "Measuring the Wind Vector Using the Autonomous Mini Aerial Vehicle M2AV," *J. Atmos. Oceanic Technol.*, 2008.

[15] WMO, "WMO Guide to Meteorological Instruments and Methods of Observations," Tech. Rep. 8, WMO, 2008.

[16] M. Jonassen, "The Small Unmanned Meteorological Observer (SUMO) Characterization and test of a new measurement system for atmospheric boundary layer research," *Master thesis at the University of Bergen, Norway*, 2008.

[17] P. Brisset, A. Drouin, M. Gorraz, P. Huard, and J. Tyler, "The Paparazzi Solution," *ENAC*, 2006.

[18] J. Reuder, M. Ablinger, H. Ágústsson, P. Brisset, S. Brynjólfsson, M. Garhammer, T. Johannesson, M. Jonassen, R. Kühnel, S. Lämmlein, T. de Lange, C. Lindenberg, S. Malardel, S. Mayer, M. Müller, H. Ólafsson, O. Rögnvaldsson, W. Schäper, T. Spengler, G. Zängl, and J. Egger, "FLOHOF 2007: An overview of the mesoscale meteorological field campaign at Hofsjökull, Central Iceland," *Meteorology and Atmospheric Physics*, vol. DOI: 10.1007/s00703-010-0118-4, 2011.

[19] S. Mayer, A. Sandvik, M. O. Jonassen, and J. Reuder, "Atmospheric profiling with the UAS SUMO: A new perspective for the evaluation of fine-scale atmospheric models," *Meteorology and Atmospheric Physics*, vol. DOI: 10.1007/s00703-010-0063-2, 2010.

[20] K. I. M. Mckinnon, "Convergence of the Nelder-Mead simplex method to a non-stationary point," tech. rep., SIAM J. Optim, 1996.

[21] J. A. Nelder and R. Mead, "A simplex algorithm for function minimization," *Computer Journal*, vol. 7, no. 4, p. 308313, 1965.

[22] H. Rachele and L. Duncan, "Desirability of using a fast sampling rate for computing wind velocity from pilot balloon data," *Monthly Weather Review*, vol. 95, no. 4, pp. 198–202, 1967.